Top Catal (2008) 50:52–65
DOI 10.1007/s11244-008-9111-2

ORIGINAL PAPER

Substituted Mo–V(Ti)–Te(Ce)-oxide M2 Catalysts for Propene Ammoxidation

Robert Häggblad · Jakob B. Wagner · Benoit Deniau · Jean-Marc M. Millet · Johan Holmberg · Robert K. Grasselli · Staffan Hansen · Arne Andersson

Published online: 23 August 2008

Abstract One of the most effective propane to acrylonitrile ammoxidation catalyst is comprised of the two phases M1 (orthorhombic) $Mo_{7.5}V_{1.5}NbTeO_{29}$ and M2 (pseudo-hexagonal) $Mo_4V_2Te_2O_{20}$. Under reaction conditions, the two phases work in symbiosis with each other where M1 is the paraffin activating component and M2 is the olefin activating component. Since the catalytic improvement of either phase should result in an enhancement of the overall acrylonitrile yield, controlled substitution of certain elements in either or both phases might result in the desired improvement. Our current study concentrates on the partial substitutions of V with Ti and Te with Ce in the M2 phase. Ti substitution results in a considerable propene activity improvement, whereas the selectivity to acrylonitrile is unaffected. Substitution with Ce, on the contrary, substantially improves the selectivity to acrylonitrile. Also, a minor improvement of the activity is notable. The acrylonitrile selectivity improvement is a result of better NH_3 utilization and comes at the expense of reduced acrolein make. XRD reveals that all of the substituted compositions retain the M2 structure and essentially are monophasic. XANES recordings show for the bulk that the Mo is 6+, the V is 4+, or 4+ and 5+ when Ce is present, the Ti is 4+, the Ce is 3+, and the Te 4+ with some 6+ also present. According to the ESR data, in the M2 with Ce (7Te/3Ce) only 21% of the V is 4+, the remainder being 5+, which tentatively can be explained by the existence of some cation vacancies in the hexagonal channels. HRTEM imaging reveals little if any differences between the materials, all have the typical pseudo-hexagonal habit of the M2 phase and expose a 1–2 nm thick surface layer without any apparent long-range ordering. XPS data show that all catalysts, including the base, are highly enriched at the surface with Te at the expense of other metals. The 7Te/3Ce composition exhibits also substantial Ce surface enrichment. Moreover, the valences of the cations at the surface differ from the bulk in that for all fresh catalysts V is 5+ and Te is 6+ on the surface. Characterization by XPS of catalysts used in propene ammoxidation, reveals reduction of Te and, except when Ce is present, also Mo. Therefore, it might be inferred that the surfaces of the catalysts studied here are comprised essentially of one or a few monolayers of TeMoO or TeCeMoO on an interacting M2 crystalline base.

R. Häggblad · J. Holmberg · A. Andersson (✉)
Department of Chemical Engineering, Lund University, Chemical Center, P.O. Box 124, 221 00 Lund, Sweden
e-mail: Arne.Andersson@chemeng.lth.se

J. B. Wagner · S. Hansen
Division of Polymer and Materials Chemistry, Department of Chemistry, Lund University, Chemical Center, P.O. Box 124, 221 00 Lund, Sweden

B. Deniau · J.-M. M. Millet
IRCELYON, Institut de Recherches sur la Catalyse et l'Environnement de Lyon, CNRS, Université Claude Bernard Lyon I, UMR5256, 2 avenue Albert Einstein, Villeurbanne, 69626 Cedex, France

Present Address:
J. Holmberg
Perstorp Specialty Chemicals AB, Perstorp Formox, 284 80 Perstorp, Sweden

R. K. Grasselli
Center for Catalytic Science and Technology, University of Delaware, Newark, DE 19716, USA
e-mail: rkgrasselli@yahoo.com

R. K. Grasselli
Department of Chemistry, Technische Universität München, 85748 Garching, Germany

Keywords Ammoxidation · Propene · Acrylonitrile · Mo–V(Ti)–Te(Ce)-oxide catalysts · M2-phase · XRD · XPS · ESR · XANES · SEM · HRTEM

1 Introduction

In recent years the Mo–V–Nb–Te-oxide system has been extensively investigated for propane oxidation [1–7] and ammoxidation [8–15] to acrylic acid and acrylonitrile, respectively. By now it is well established that the catalyst system comprises the two orthorhombic phases denoted M1 and M2 (pseudo-hexagonal) [16, 17] with the respective general composition $(TeO)_{2-2x}(Te_2O)_xM_{20}O_{56}$ ($0 \leq x \leq 1$, M = Mo, V and Nb) and $(TeO)_2M_6O_{18}$ (M = Mo, V and either with or without Nb) [18, 19]. The M1 phase is active and selective for the conversion of propane to acrylic acid [7, 13] and acrylonitrile [11, 13, 14], whereas the M2 phase is almost inactive for propane conversion, though active and selective for the corresponding conversions of propene [11, 14, 20]. For the conversion of propene to acrylonitrile we have found that the M2 phase is more selective than M1 and demonstrated that the best catalyst for propane ammoxidation is an intimate mixture of both phases [14]. The symbiosis between the phases can be explained by intermediate propene, formed from propane on M1, being allowed to readsorb on M2, where it is selectively transformed to acrylonitrile.

Recently, we have succeeded to substitute in M2 various amounts of W for Mo, Ti for V, Nb for Mo and V, Fe for V and Ce for Te [21]. The preparations are active and selective for the ammoxidation of propene. Substitution in M2 is of interest, not only because M2 together with M1 are components in propane ammoxidation catalysts, but also because M2 is a candidate catalyst for propene ammoxidation. In our previous work [21] we observed that partial replacement of V by Ti in M2, gives a significant increase of the specific acitivity for propene ammoxidation, whereas the selectivities to acrylonitrile and acrolein are largely unaffected. On the other hand, substitution of Ce for 30% of Te gives increased activity and improved selectivity to acrylonitrile at the expense of acrolein. Especially, the observation that Ti substitution increases the activity of M2 is remarkable as the reverse was expected considering that vanadia commonly is active for catalytic oxidations, whereas titania is used as an almost inactive support. To elucidate the causes of the catalytic effects of Ti and Ce substitutions in M2, the present study was undertaken, dealing with detailed characterizations of the substituted compounds using electron microscopy, ESR, XANES and XPS.

Table 1 Notation, metal composition, and specific surface area of the prepared samples

Catalyst notation	Metal composition (at.%)	Specific surface area (m^2/g)
M2-0	$Mo_{47}V_{25}Te_{28}$	1.3
VT-30	$Mo_{47}V_{17}Ti_8Te_{28}$	1.0
VT-50	$Mo_{47}V_{13}Ti_{13}Te_{28}$	0.8
TC-30	$Mo_{47}V_{25}Ce_9Te_{20}$	0.7

2 Experimental

2.1 Catalyst Preparation

The M2-type phases were prepared from $(NH_4)_6Mo_7O_{24} \cdot 4H_2O$, NH_4VO_3, H_6TeO_6, TiO_2, and $Ce(NO_3)_3 \cdot 6H_2O$, which in desired amounts were dissolved in water at 60 °C. The water in the prepared solutions was then evaporated during 4 h in an oven kept at 150 °C. The obtained precursors were subsequently calcined in two steps to give the correct phase. First, the precursors were calcined in air at 275 °C for 2 h and then, for another 2 h under a flow of argon in a quartz reactor held at 550 °C. The nominal compositions of the prepared samples and their notations are given in Table 1. Compared to the unsubstituted M2 sample, denoted M2-0; in the VT-30 and VT-50 samples 30% and 50%, respectively, of the V was replaced by Ti, whereas in TC-30, 30% of the Te was replaced by Ce.

2.2 Catalyst Characterization

The specific surface areas of the catalysts were measured on a Micromeritics Flowsorb 2300 instrument. All samples were degassed at 200 °C for 24 h before analysis.

X-ray powder diffraction (XRD) analysis was performed on a Seifert XRD 3000 TT diffractometer using monochromatic Cu Kα radiation and a rotating sample holder. The instrument was calibrated using a silicon standard.

Scanning electron microscopy (SEM) images were acquired with a Jeol 6700F microscope. The acceleration voltage was set to 5 kV and the working distance to 8 mm. For high-resolution imaging (HRTEM), the samples were studied in a Jeol 3000F FEG transmission electron microscope operated at 300 kV and equipped with a CCD for image acquisition.

XPS analyses were made on a Kratos AXIS 165 instrument using monochromatic Al Kα X-ray radiation (1486.58 eV). The C 1 s signal was used as a reference peak and was set to a binding energy of 284.8 eV. The experimental data were analysed using the CasaXPS software, and the quantifications were made using a linear background. All measurements were made on pellets.

Electron spin resonance (ESR) spectra were recorded using a Bruker ELEXSYS 500 spectrometer operating in the Q-band mode (9.4 GHz). Vanadyl sulfate dispersed in silica was used for spin calibration. Samples of ca. 15 mg were placed inside a quartz probe cell and analyzed at 100 K. The EPR data were directly fed into a PC to be processed as desired.

The XANES measurements were performed at the I811 beamline at MAX-lab (Lund University) using a Si(111) double crystal monochromator and three ionisation chambers (Oxford-Danfysik). Spectra of V, Te, Ti and Ce were recorded in transmission mode. The sample was positioned between the first and second ionisation chamber, while a reference foil was positioned after the sample, between the second and third ionisation chamber. XANES spectra were recorded for the V K-, Te L_3-, Ti K- and Ce L_3-edges using V, Ti, Ti and Cr foils, respectively, as energy references. For the measurements, the samples were ground and diluted with boron nitride to give an appropriate element concentration. Spectra of the Mo L_3-edge were recorded in fluorescence mode using an energy-dispersive solid-state silicon-drift detector (Vortex 90-EX, SII Nano Technology), which was positioned perpendicular to the incoming beam. The sample was positioned after the first ionisation chamber, 45 degrees to both the incoming beam and the detector. No reference foil was used for online energy calibration. Instead, a Mo foil was measured between every second sample recorded. No change in energy was observed in the different scans. To prevent self absorption, carefully ground undiluted samples mounted on tape were used for the fluorescence measurements.

2.3 Activity Measurements

The prepared catalysts were tested for the ammoxidation of propene at atmospheric pressure using a plug-flow microreactor made of stainless steel. To obtain isothermal conditions, the reactor was embedded in an aluminium block and placed in a tube furnace. The activity measurements were performed at 400 °C with the feed composition 6.0 vol.% propene, 6.9 vol.% ammonia, 17.8 vol.% oxygen and 69.3 vol.% argon. Catalytic data were collected for different space velocities by varying the catalyst load and/or the total flow rate, giving the selectivity variations with the degree of conversion and allowing calculation of the activity at the defined inlet conditions. The catalyst load was 0.50–2.50 g, and the total flow of propene, ammonia, oxygen and argon was varied between 10.2 and 23.1 Ncm^3/min. Propene, acrylonitrile, acetonitrile, acrolein and CO_2 were analysed online using a gas chromatograph, which was equipped with an FID detector, a TCD detector and a Haysep Q column. The CO was analysed online with a Rosemount Binos 100 IR instrument.

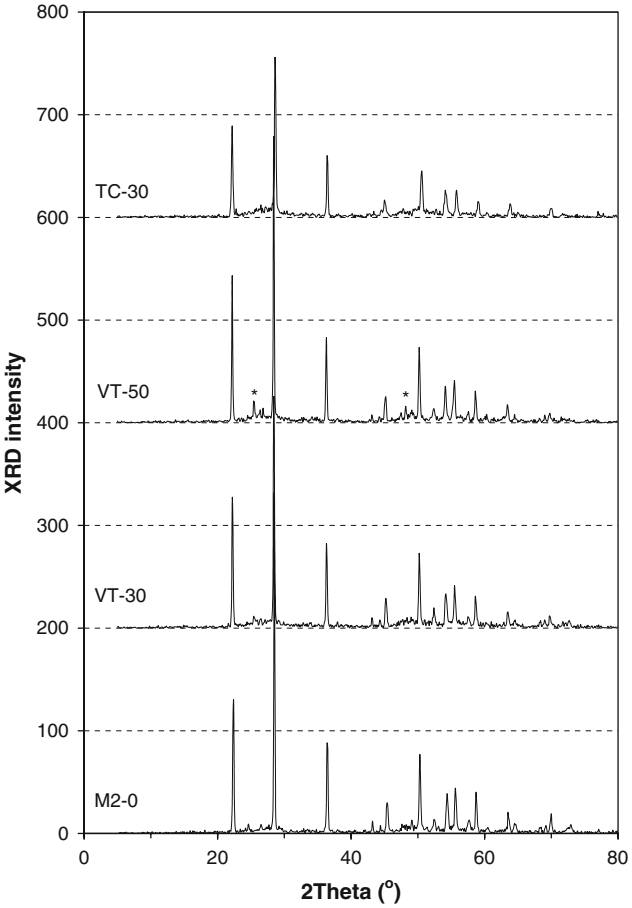

Fig. 1 X-ray diffractograms of the prepared catalysts. See Table 1 for notation and composition. Peaks marked by (*) in the diffractogram of VT-50 are from TiO_2 (anatase)

3 Results

3.1 X-ray Diffraction

The X-ray diffraction patterns of the catalysts in Fig. 1 reveal that M2-0, VT-30 and TC-30 are single phase preparations consisting of orthorhombic (pseudo-hexagonal) M2-type phases [17, 19, 21, 22]. The VT-50 sample, on the other hand, is almost monophasic but shows minor peaks at $2\theta = 25.2°$ and 48.0°, which are the two strongest reflections from the anatase form of TiO_2, JCPDS file no. 21-1272 [23]. In our previous work [21] we reported that the compositions of VT-50 and TC-30 correspond to the limits for replacement of V and Te by Ti and Ce, respectively, and that the variation of the lattice parameters with the degree of substitution follows Vegard's law.

3.2 Catalytic Performance

Activity and selectivity data for the prepared catalysts are shown in Fig. 2. Considering the data for the M2-0, VT-30

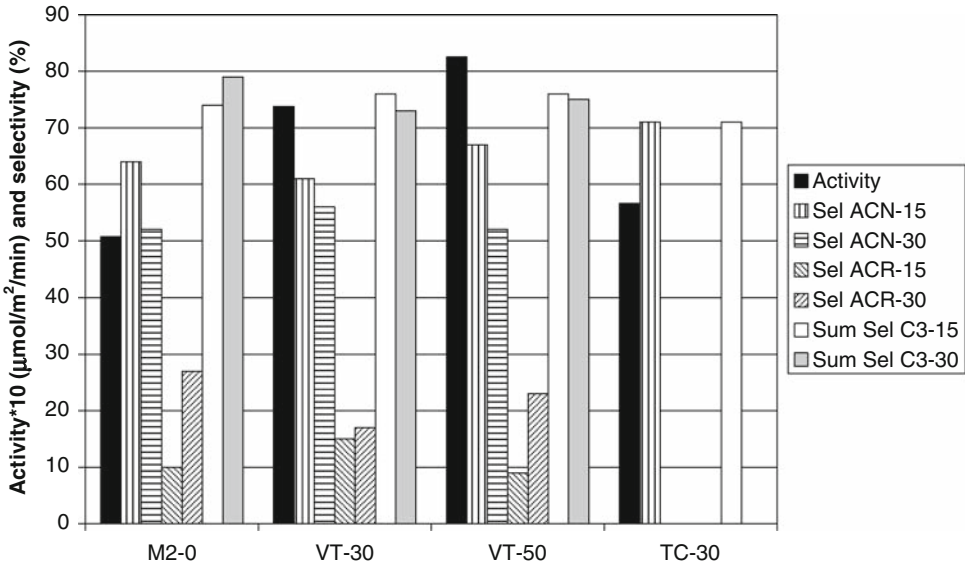

Fig. 2 Propene ammoxidation over unsubstituted M2 (denoted M2-0), Ti-substituted (VT-30, VT-50) and Ce-substituted (TC-30) M2-type phases. Specific reaction rates and selectivities for the formation of acrylonitrile (Sel ACN), acrolein (Sel ACR) and the sum thereof (Sum Sel C3) at 15% and 30% of propene conversion. Reaction conditions: 400 °C and feed composition 6.0 vol.% propene, 6.9 vol.% ammonia, 17.8 vol.% oxygen and 69.3 vol.% argon

and VT-50 samples, it is seen that the surface area normalised activity increases with the degree of substitution of Ti for V, whereas the selectivities to acrylonitrile, acrolein and the sum thereof are almost the same for the samples. Moreover, the data show that the selectivity to acrylonitrile decreases with an increase of the propene conversion, while concurrently the selectivity to acrolein increases. The sum of the two C_3 product selectivities is approximately constant and is in the order of 75%.

The data in Fig. 2 for TC-30 show that the replacement of some of the Te by Ce gives a 10% increase in activity compared to the unsubstituted M2-0. A more apparent effect of Ce substitution is that the selectivity to acrylonitrile is increased and no acrolein is formed on TC-30. At 15% propene conversion the selectivities to acrylonitrile and acrolein are 64% and 10% on M2-0, and for TC the corresponding data are 71% and 0%, respectively.

3.3 XPS Characterization

The metal surface compositions of the prepared catalysts were determined by XPS analysis. The results are summarized in Table 2 and show for all catalysts an enrichment of Te at the surface, and for TC-30 also of Ce, at the expense of the other metals. However, compared with the V and Ti contents, the relative decrease of the Mo content is smaller. After use of the catalysts in propene ammoxidation, the XPS analyses show only minor changes of the metal composition at the surface.

XPS spectra of the Mo 3d region are displayed in Fig. 3. The spectra for the freshly prepared M2-0 show symmetric $3d_{3/2}$ and $3d_{5/2}$ peaks at 236.0 and 232.8 eV, respectively, which are from Mo^{6+} [3, 19, 24]. VT-30 and VT-50 show shoulders on the low energy side of the 3d peaks, which grow in size with the Ti content. The $3d_{3/2}$ and $3d_{5/2}$ shoulder peaks are at 234.8 and 231.5 eV, which can be assigned to the Mo^{5+} state [19, 24]. After the samples being used in propene ammoxidation, the proportion of Mo^{5+} has increased. The fraction $Mo^{5+}/(Mo^{6+} + Mo^{5+})$ in the catalysts are given in Table 2 as determined by peak deconvolution.

For TC-30, the spectrum of the Mo 3p region in Fig. 3 is practically the same before and after use in propene ammoxidation. The $3p_{1/2}$ and $3p_{3/2}$ peaks at 416.0 and 398.5 eV, respectively, are single peaks and can be assigned to Mo^{6+}.

The XPS spectra of the V 2p region were very similar for all catalysts. The binding energies of the $2p_{1/2}$ and $2p_{3/2}$

Table 2 Metal compositions as determined by XPS before and after use in propene ammoxidation

Catalyst	Nominal metal composition (at.%)	Fresh catalyst		Used catalyst			
		Surface composition (at.%)	Mo^{5+}/Mo (%)	Surface composition (at.%)	Mo^{5+}/Mo (%)	Te^{4+}/Te (%)	Te^{2+}/Te (%)
M2-0	$Mo_{47}V_{25}Te_{28}$	$Mo_{40}V_{13}Te_{46}$	0.0	$Mo_{41}V_{13}Te_{46}$	1.7	4.4	3.5
VT-30	$Mo_{47}V_{18}Ti_8Te_{28}$	$Mo_{41}V_{11}Ti_4Te_{44}$	3.7	$Mo_{43}V_9Ti_3Te_{44}$	10.0	0.0	2.5
VT-50	$Mo_{47}V_{13}Ti_{13}Te_{28}$	$Mo_{42}V_8Ti_5Te_{46}$	7.5	–	–	–	–
TC-30	$Mo_{47}V_{25}Ce_8Te_{20}$	$Mo_{43}V_{15}Ce_{11}Te_{31}$	0.0	$Mo_{43}V_{13}Ce_{11}Te_{33}$	0.0	7.1	0.0

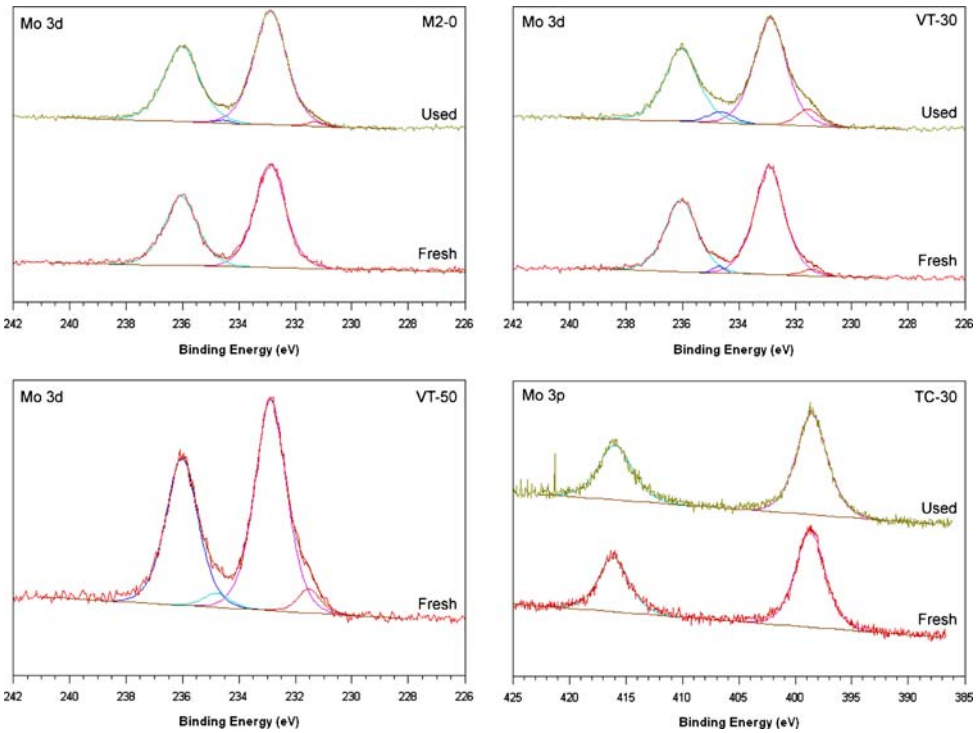

Fig. 3 XPS spectra of the Mo 3d region for M2-0, VT-30 and VT-50, and the Mo 3p region for TC-30. The used samples were analysed after use in propene ammoxidation

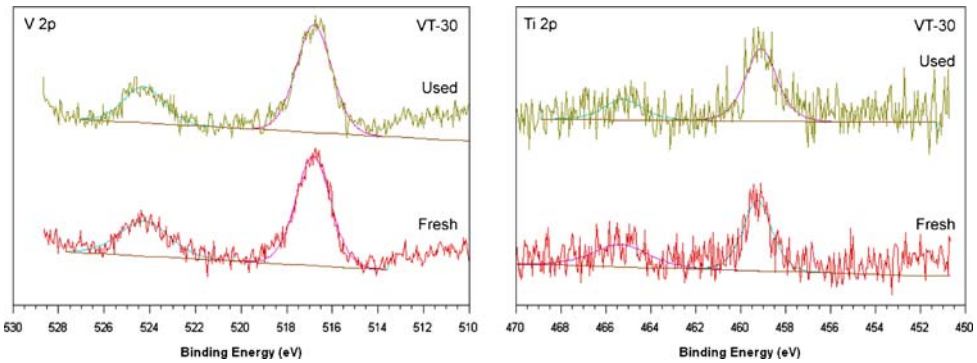

Fig. 4 XPS spectra for VT-30 of the V 2p and Ti 2p regions before and after use of the sample in propene ammoxidation

peaks were 524.2–524.3 eV and 516.8–517.0 eV, respectively. As a typical example the spectra for VT-30 are shown in Fig. 4. No change in either peak shape or position was observed after the samples were used in ammoxidation. Considering that the width of the $2p_{3/2}$ peaks at half maximum was in all cases $\sim$1.6 eV, it can be concluded that it is a single peak. By comparison with the binding energies reported in the literature for vanadia and reduced vanadia [25, 26], the binding energy measured here for the $2p_{3/2}$ peak suggests that the V at the surface is pentavalent.

The Ti 2p spectrum in Fig. 4 for the freshly prepared VT-30 shows Ti $2p_{1/2}$ and Ti $2p_{3/2}$ peaks at 465.4 and 459.1 eV, respectively, which can be assigned to Ti^{4+} [27]. No difference in the oxidation state of Ti is noticeable after the sample has been used in ammoxidation as the spectrum for the corresponding used sample shows. VT-50 shows the same spectral features as VT-30 in the Ti 2p region.

In Fig. 5 are presented the Te 3d spectra for M2-0, VT-30 and TC-30. All fresh catalysts, including VT-50, showed single featured Te $3d_{3/2}$ and Te $3d_{5/2}$ peaks at 587.0–587.1 eV and 576.6–576.8 eV, respectively, which can be assigned to Te^{6+} [18]. Reduction of Te is observed after the samples have been used in propene ammoxidation. In addition to the Te $3d_{5/2}$ main peak at $\sim$576.7 eV, M2-0 exhibits two additional peaks at 574.9 and 573.4 eV. The latter two peaks are possibly derived from Te^{4+} and Te^{2+} states. VT-30 and TC-30 show each only one of the peaks from reduced Te at 573.4 and 574.7 eV, respectively. The relative contents of Te^{4+} and Te^{2+} are given in Table 2, where it is seen after use in ammoxidation that the VT-30 has a lesser amount of reduced Te species compared to M2-0 and TC-30. Of the latter samples, M2-0 shows the severest reduction with the formation of not only Te^{4+} but also Te^{2+}.

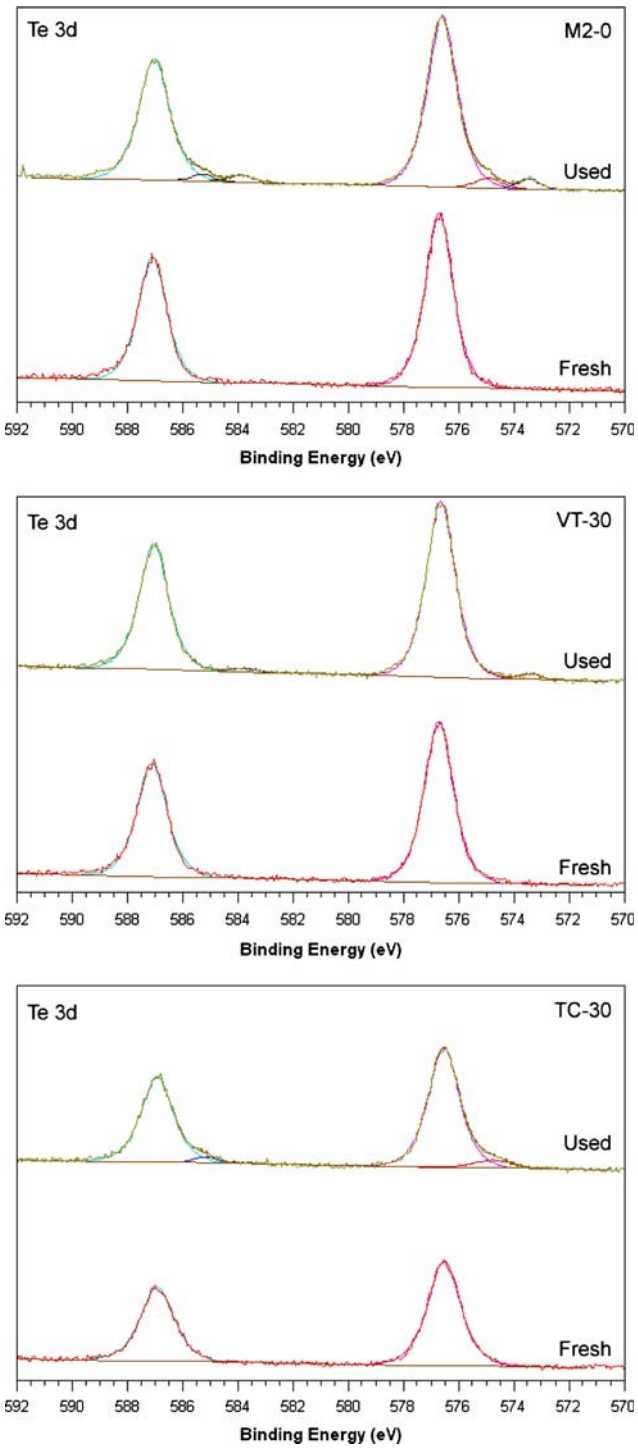

Fig. 5 XPS spectra of the Te 3d region for M2-0, VT-30 and TC-30 before and after use in propene ammoxidation

The XPS spectra of the Ce 3d region for fresh and used TC-30 are displayed in Fig. 6. The two spectra are very similar. Each spectrum consists of two components with maxima at 904.1 and 899.8 eV for Ce $3d_{3/2}$ and 885.7 and 881.8 eV for Ce $3d_{5/2}$, which all can be assigned to Ce^{3+} in agreement with published data for Ce_2O_3 and $CeVO_4$ [28].

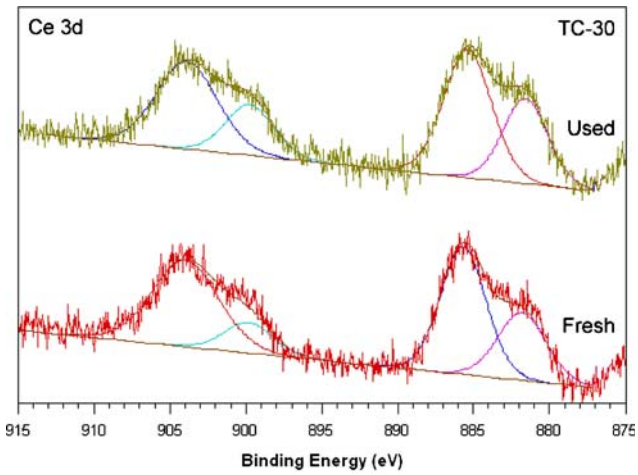

Fig. 6 Ce 3d XPS spectra for TC-30 before and after use in propene ammoxidation

In the order of decreasing energy, the four peaks have been denoted u′, u_o, v′ and v_o, respectively [29, 30]. The Ce $3d_{5/2}$ peaks v_o and v′ have been assigned to the $3d^94f^2(O\ 2p^5)$ and $3d^94f^1(O\ 2p^6)$ Ce(III) final states, respectively [29], and the corresponding Ce $3d_{3/2}$ u_o and u′ features can be assigned similarly.

3.4 XANES Characterization

The valences of the metals in the bulk phases were determined by XANES measurements. Figure 7a shows the Mo L_3-edge spectra of the M2-type catalysts and the reference compounds MoO_2 and MoO_3. All samples show a significant white line and a doublet peak above the edge. The edge position for MoO_2 and MoO_3 is 2522.0 and 2523.8 eV, respectively. Also, the two reference compounds show different doublet features. For MoO_2, the second peak from the edge is more intense than the first peak, whereas the opposite is observed for MoO_3. The catalyst preparations all show the same edge feature, which is similar to that for MoO_3. For M2-0, VT-30 and TC-30 the edge position is 2524.1 eV and somewhat lower 2523.5 eV for VT-50. Still, the edge positions as well as the edge features suggest that the Mo predominantly is hexavalent in the M2-type preparations.

In Fig. 7b are shown the V K-edge spectra of the M2-type catalysts and the reference compound V_2O_5. The pre-edge position 5467.1 eV is the same for all catalysts, whereas for V_2O_5 it is 5468.3 eV. Also, there is a corresponding difference in the main edge positions. A shift of 1.2 eV towards lower energy compared to V_2O_5 is in agreement with the V in the catalysts being tetravalent [19], which also agrees with bond valence calculations [17]. Compared with M2-0 and the Ti substituted catalysts, TC-30 shows a broadening of the pre-edge peak towards

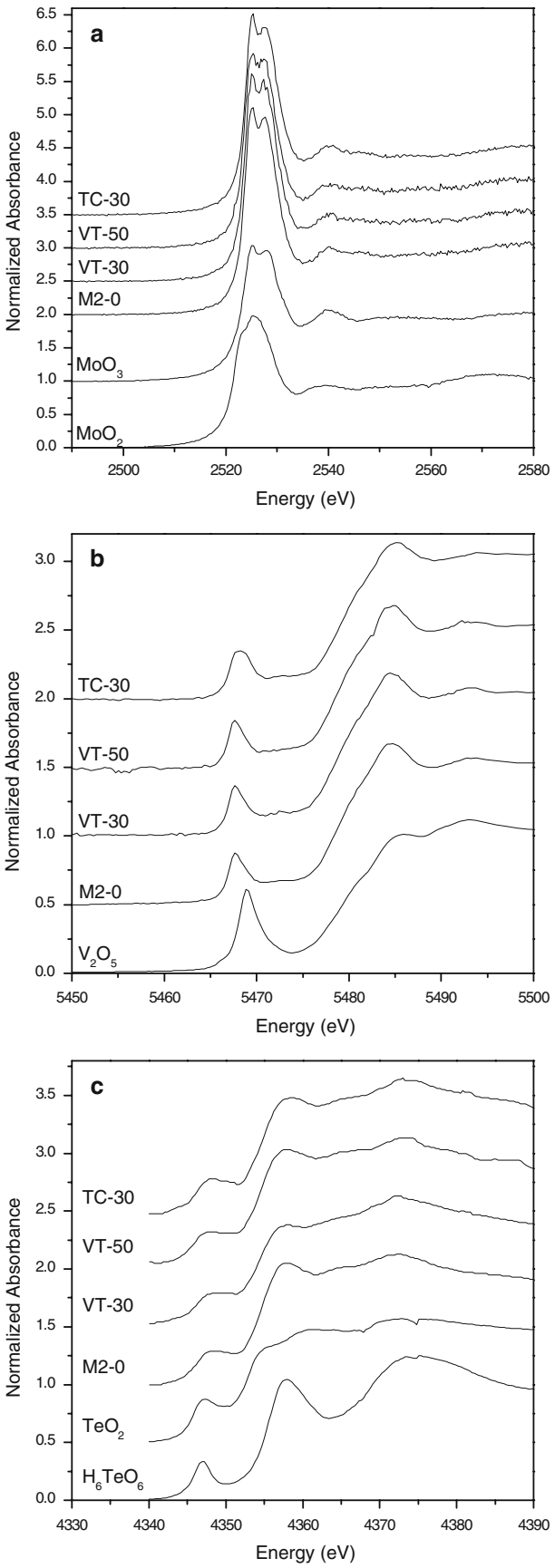

◀ **Fig. 7** Normalized Mo L_3-, V K- and Te L_3-edge XANES spectra of catalysts and reference compounds. (**a**) Mo L_3-edge spectra for MoO_2, MoO_3, M2-0, VT-30, VT-50 and TC-30; (**b**) V K-edge spectra for V_2O_5, M2-0, VT-30, VT-50 and TC-30; and (**c**) Te L_3-edge spectra for H_6TeO_6, TeO_2, M2-0, VT-30, VT-50 and TC-30

the high energy side, possibly indicating the presence of both V^{4+} and V^{5+} in the sample.

As displayed in Fig. 7c, Te shows unchanged L_3 pre-edge and main edge positions when substituting partially Ti for V and Ce for Te. The main edge position for M2-0 as well as VT-30, VT-50 and TC-30 is 4354.5 eV. The edge position of the two reference compounds Te(IV)O_2 and H_6Te(VI)O_6 is 4353.2 and 4355.6 eV, respectively, i.e., the main edge position of Te in the M2-type catalysts is in between those for the reference compounds, indicating two types of Te in the catalysts, namely Te^{6+} and Te^{4+} [31].

The Ti K-edge spectra for VT-30, VT-50 and TiO_2 (anatase) are displayed in Fig. 8a, showing complex pre-edge features in agreement with previous results [32]. The main edge position of the reference compound TiO_2 is 4984.9 eV and as it is the same for VT-30 and VT-50, it can be concluded that the Ti is tetravalent in the Ti substituted catalysts.

Figure 8b shows the Ce L_3-edge spectra for TC-30 and the reference compound CeO_2. The spectrum for TC-30 shows a strong white line with the edge positioned at 5724.1 eV, whereas the spectrum for CeO_2 is very different displaying a doublet feature with the edge at 5725.3 eV. The spectra recorded for TC-30 and CeO_2 are very similar to previously published spectra for compounds with trivalent and tetravalent Ce, respectively, with regard to both the edge position as well as the edge and post edge features [33, 34]. Thus, it can be safely concluded that Ce in the bulk TC-30 is trivalent.

3.5 Electron Microscopy

The catalysts were studied by SEM to address the morphology of the samples. The SEM micrographs in Fig. 9 reveal the morphology of the primary particles to be more rounded in the substituted samples than in the unsubstituted M2-0. Furthermore, the size of the primary particles is of the order 100–300 nm in the substituted samples, which is approximately a factor of two smaller than for the M2-0 sample. In all samples the particles form agglomerates of several microns. No distinct differences are observed in the morphology for the substituted samples, although the VT-50 sample contains some spherical particles, which might be the TiO_2 observed in the XRD.

Figure 10 shows a high resolution TEM image of M2-0 revealing the lattice fringes corresponding to the $(40\bar{1})$ and

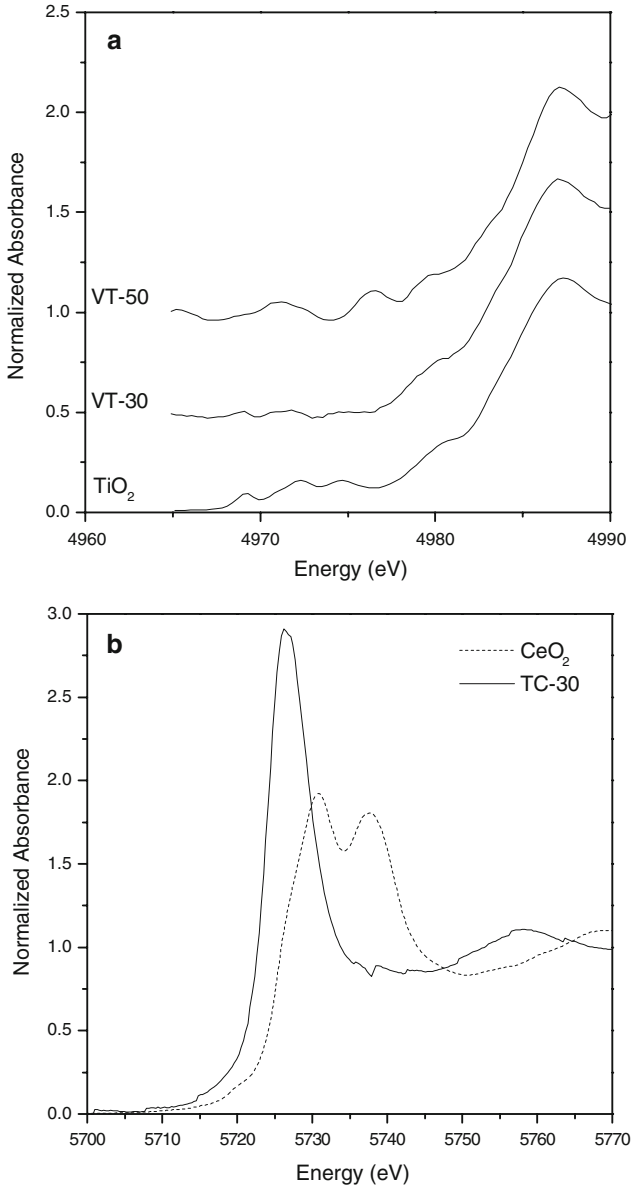

Fig. 8 Normalized Ti K- and Ce L_3-edge XANES spectra of catalysts and reference compounds. (**a**) Ti K-edge spectra for TiO_2, VT-30 and VT-50; and (**b**) Ce L_3-edge spectra for CeO_2 and TC-30

the (010) planes. This implies that the crystal is viewed along the [104] zone axis.

In Fig. 11 a high resolution TEM image shows a VT-30 crystal. The distance between the lattice fringes and their mutual angles coincides with that of M2 viewed along the [101] zone axis. The lattice fringes are not observed in the outer few nanometres of the crystal, indicating a reconstruction of the surface. As the sample has to be electron transparent to reveal lattice fringes, only the thinner parts of the crystal are shown.

The TC-30 crystal shown in Fig. 12 is oriented along the [110] axis of the M2 crystal structure. The projected structure of the surface (slightly underfocused) shows a thin 1–2 nm layer of material without any apparent long-range ordering.

3.6 Catalyst Characterization with ESR

The M2-type preparations were characterized by ESR at 100 K. The spectra in Fig. 13 show two signals, one which is characterized by a hyperfine splitting multiplet due to the ^{51}V nucleus (I = 7/2, 99.76%) and another one characterized by a broad isotropic line. The calculated g and A parameters of the V^{4+} signals are given in Table 3. The multiplet signal corresponds to well-isolated vanadyl species in distorted octahedral environment, whereas the isotropic signal indicates the presence of interacting vanadyl species [35]. The isotropic signal includes a small contribution from the Mo^{5+} species detected at the surface by XPS (Table 2) which are also active in ESR.

The overall intensities of the ESR spectra were measured and compared to that of a standard $VOSO_4$–SiO_2 mixture to determine the density of spins in each compound. The relative number of spins corresponding to each of the two types of species was determined by deconvolution of the two-signal spectra. The data are included in Table 3, and in Fig. 14 are plotted the total number of spins versus the number of vanadium atoms in the prepared catalysts. For M2-0, VT-30 and VT-50 one may observe a linear relationship passing through the origin. The slope of the curve is 0.974 spin/V atom, confirming the XANES data that virtually all V in these samples is tetravalent. As expected, the relative proportion of isolated V^{4+} species increases with decreasing total V content (Table 3). For TC-30, on the other hand, the data in Fig. 14 corresponds to only 21% of the V in the sample being tetravalent.

4 Discussion

4.1 Substitutions in M2

The stoichiometry of the orthorhombic, pseudo-hexagonal M2 phase can be written $(TeO)_2M_6O_{18}$ with M = Mo, V and either with or without Nb [19]. The structure, which is depicted in Fig. 15, is built up of layers with corner-sharing MO_6 octahedra to form 3- and 6-membered rings on (001). As the layers are connected by corner-sharing along [001], hexagonal channels are formed being occupied by interconnected Te–O units forming infinite chains in the c-direction [17, 18]. The successful substitution in M2 of V with Ti and Te with Ce is confirmed by the XRD patterns in Fig. 1, showing that M2-0, VT-30 and TC-30 are essentially phase pure samples consisting of M2-type phases. Characterization of the samples with HRTEM (Figs. 10–12) confirms that they are pure phases. However,

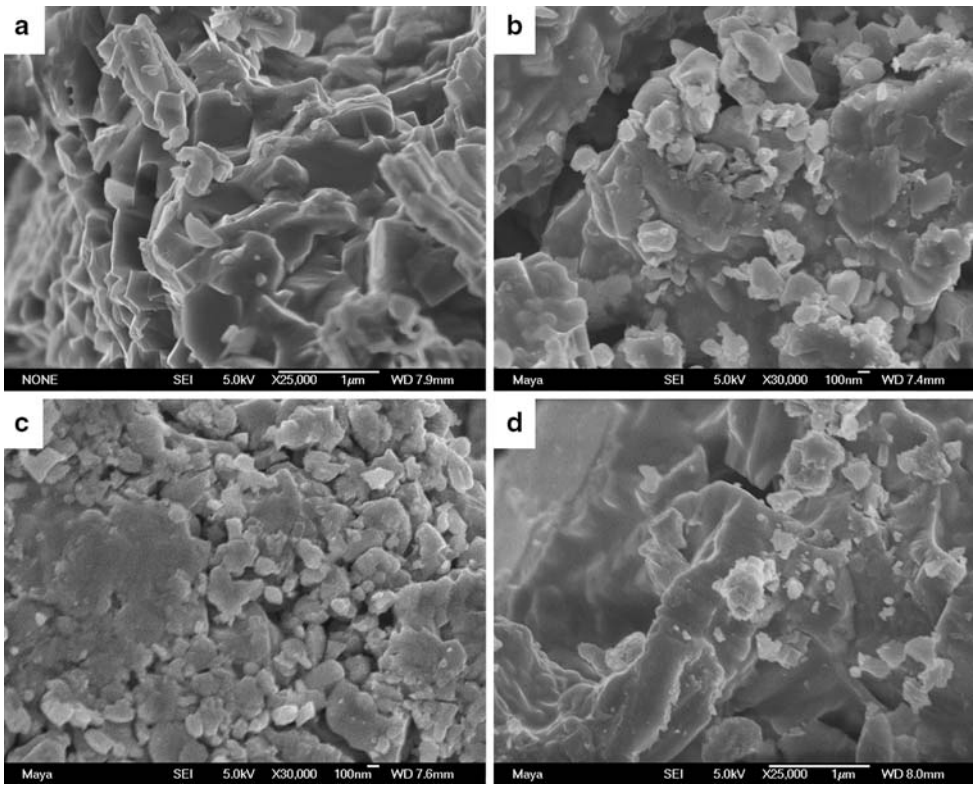

Fig. 9 SEM images of the unsubstituted catalyst M2-0 (**a**) and the substituted catalysts VT-30 (**b**), VT-50 (**c**), and TC-30 (**d**)

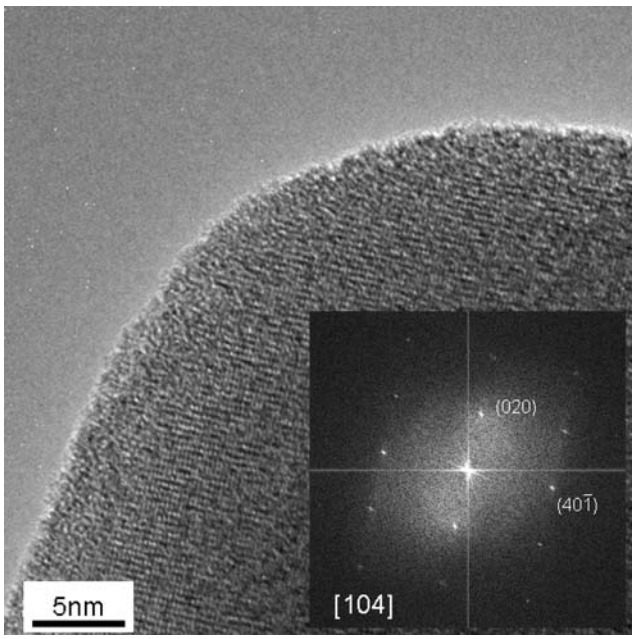

Fig. 10 Lattice fringe TEM image of M2-0, showing a crystal oriented in the [104] zone axis. Inset: Fourier Transform of the image

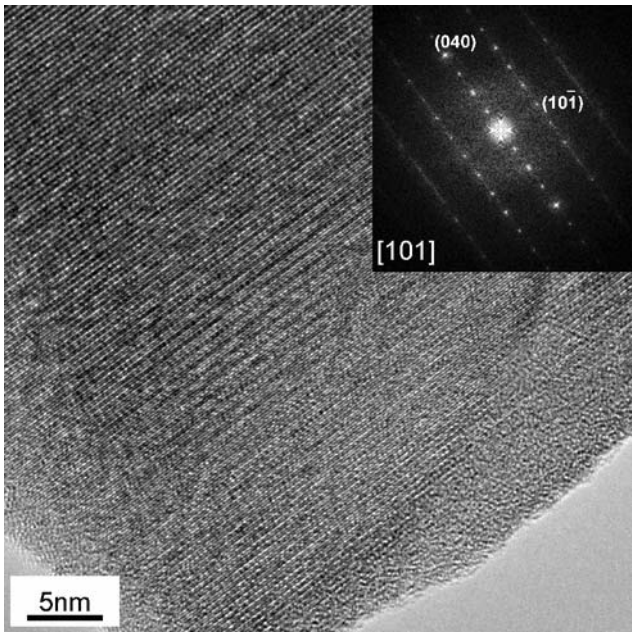

Fig. 11 Lattice fringe TEM image of VT-30, showing a crystal oriented in the [101] zone axis. Inset: Fourier Transform of the image

in the XRD of VT-50 weak peaks from TiO_2 (anatase) are noticeable, which is confirmed by HRTEM imaging. Yet, the amount of titania must be small as the lattice parameters vary linearly with the degree of Ti-substitution up to and including 50% replacement of V [21]. Also, both XRD and electron microscopy showed no sign of formation of any Mo–Te-oxide in VT-50. The successful substitution of Ti for almost 50% of the V in M2, is in agreement with the ESR spectra in Fig. 13 and the data in Table 3, showing that the partial substitution of V with Ti results in the

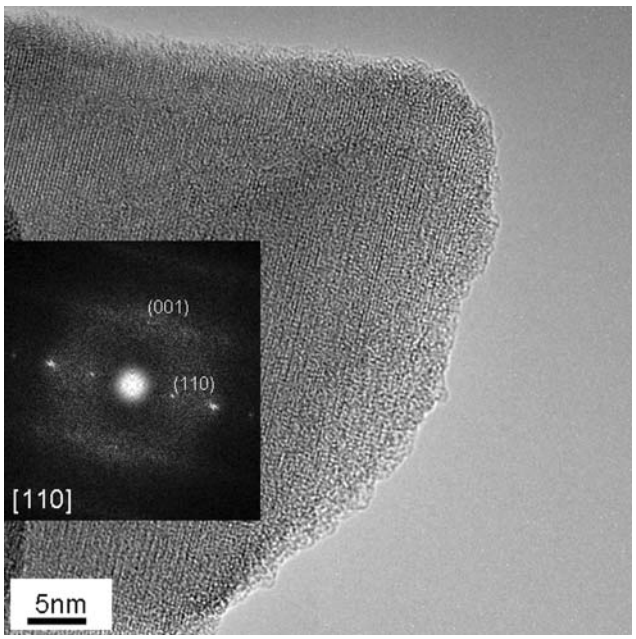

Fig. 12 Lattice fringe TEM image of TC-30, showing a crystal oriented in the [110] zone axis. Inset: Fourier Transform of the image

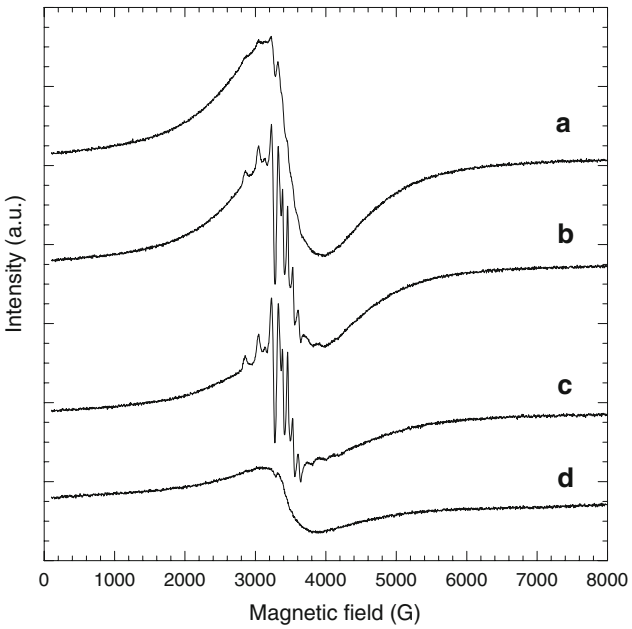

Fig. 13 ESR spectra at 100 K for freshly prepared catalysts M2-0 (a), VT-30 (b), VT-50 (c) and TC-30 (d)

relative intensity of the hyperfine signal being increased as is the relative amount of isolated V^{4+} species. The fact that the ionic radii for 6-coordinated V^{4+} and Ti^{4+} are very close in size 0.72 and 0.74 Å, respectively [36], is in agreement with the observed substitution.

Bond valence sum calculations indicate that the formal valences of the cations in the bulk are Mo^{6+}, V^{4+}, Nb^{5+} and Te^{4+} in an unsubstituted Nb-containing M2 with the composition $Mo_{4.31}V_{1.36}Nb_{0.33}Te_{1.81}O_{19.81}$ [17]. From combined XANES, Mössbauer, ESR and chemical analysis data, the formula for a Nb-free M2 was derived to be $(Te^{IV}O)_{2.1}V_{1.5}{}^{IV}V_{0.2}{}^{V}Mo_{0.8}{}^{V}Mo_{3.5}{}^{VI}O_{18}$ [19]. According to the Mo L_3-edge XANES spectra in Fig. 7a for the unsubstituted and substituted M2-type phases, the Mo is hexavalent in the bulk. The XANES spectra in Fig. 7b show that the V in the bulk is tetravalent in M2-0 and the Ti substituted VT-30 and VT-50; which is further confirmed by the plot of ESR data for the same samples (Fig. 14). Conversely, for TC-30, the ESR data in Table 3 and Fig. 14 show that only about 20% of the V is tetravalent in this sample. In support of this finding is the V K-edge spectrum for TC-30 in Fig. 7b showing a pre-edge peak that is broader than the corresponding peaks for the other samples, confirming the presence of both V^{4+} and V^{5+} in TC-30. When contemplating the valences of the metals, it should be noted that the structure of M2 is related to that of the hexagonal tungsten bronzes $(Me)_xW_3O_9$ with Me = K, Rb or Cs, where x is variable and has an upper limit of one [37]. For $x = 1$, the valence formula becomes $Me^{I}W^{V}W_2{}^{VI}O_9$ with all the hexagonal channel sites being occupied by the alkali metal, whereas completely empty channels correspond to $W_3{}^{VI}O_9$. In the related M2 phase with hexavalent Mo, channels completely filled with chains of interconnected $[Te^{IV}–O]^{2+}$ units correspond to $(Te^{IV}O)V^{IV}Mo_2{}^{VI}O_9$. As the Ce L_3-edge spectrum for TC-30 in Fig. 8b unequivocally shows that the Ce is trivalent, the observation of both V^{5+} and V^{4+} in TC-30 can in part be explained by the existence of the chains in the hexagonal channels containing $[Ce^{III}–O]^{+}$ units corresponding to the

Table 3 The g and A parameters of the V^{4+} signals of the M2-type catalysts, total number of spins and relative amount of isolated V^{4+} species

Catalyst	Signal	g	$g_{\|\|}$	$g_{\perp}$	$A_{\|\|}$ (G)	$A_{\perp}$ (G)	Total number of spins (10^{20} spin/g)	Relative amount of isolated V^{4+} (%)
M2-0	Isotropic	1.975					11.28	<0.005
VT-30	Isotropic multiplet	1.975	1.911	2.010	196.7	72.5	8.00	0.059
VT-50	Isotropic multiplet	1.976	1.910	2.008	195.4	74.2	5.86	0.102
TC-30	Isotropic	1.974					2.37	

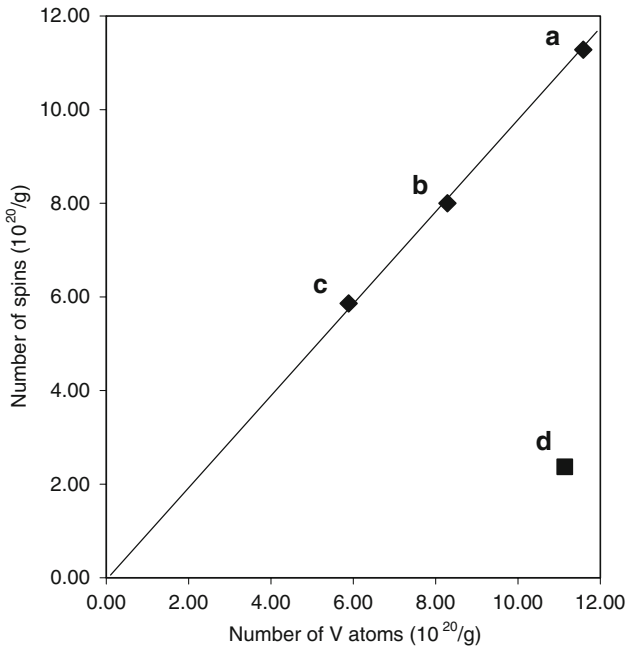

Fig. 14 Number of spins, as determined by integration of ESR signals, as a function of the vanadium content of the samples M2-0 (a), VT-30 (b), VT-50 (c) and TC-30 (d)

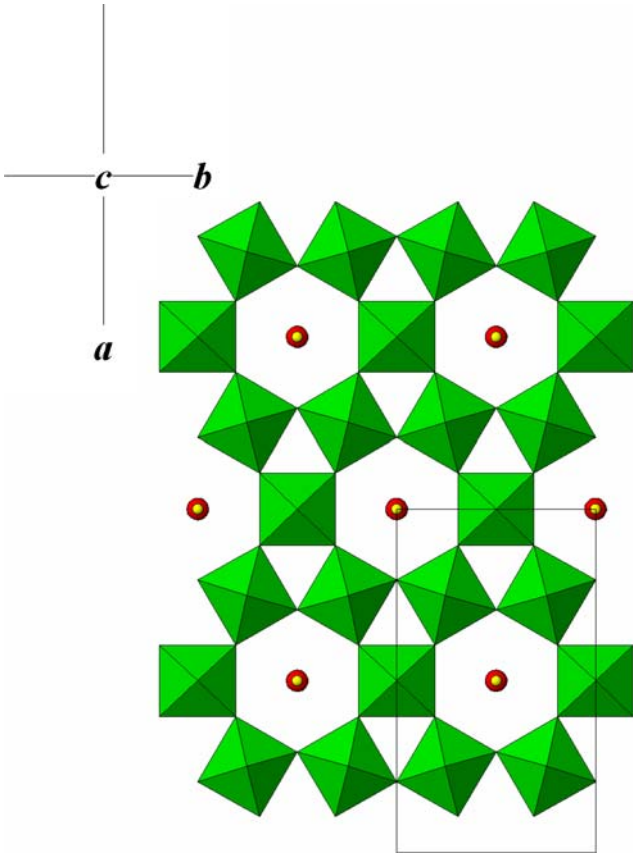

Fig. 15 The crystal structure of the M2-phase. Green oxide ion octahedra centered by transition metal ions (Mo, V, Ti). Idealized position for Te and Ce ions (red) and oxide ion (yellow) in the channels

stoichiometry $(Ce^{III}O)V^{V}Mo_2{}^{VI}O_9$. Thus, one Ce^{3+} should generate one V^{5+}. Considering that only 30% of the Te has been replaced by Ce, the fact that the V^{5+} content is higher than that of Ce^{3+} (Table 1) indicates that some of the hexagonal channel sites can be vacant in agreement with previous observations [17]. Compared with Te^{4+}, which in M2 is coordinated to four oxygen atoms of which two are in the channel and two are shared with 6-coordinated metals [17, 18], Ce^{3+} prefers either 6- or 8-coordination. Therefore, Ce^{3+} should be expected to be located closer to the center of the hexagonal channel in line with 8-coordinated Ce^{3+} (1.28 Å [36]), being similar in size to the corresponding La^{3+} (1.30 Å [36]), which has been found to be positioned exactly in the channel center in the structure-related compound La_xWO_{3+y} with $x \approx 0.10$ and $y \approx 0.15$ [38]. As Ce^{3+} is a larger cation than Te^{4+}, channels with Ce should have some vacancies. Considering that such vacancies should generate V^{5+} on behalf of V^{4+}, it must be cation positions that are vacant and not oxygen positions. Hypothetical chain terminations of the type –O–Ce–O □ O–Te–O– can exist where □ is a cation vacancy in the tunnel. Each vacancy generates one $(Ce^{III}O_{1.5})Mo_3{}^{VI}O_9$, one □ $Mo_3{}^{VI}O_9$ and one $(Te^{IV}O_{1.5})V^{V}Mo_2{}^{VI}O_9$, and where each of the two former units gives one $(Te^{IV}O)V_2{}^{V}Mo^{VI}O_9$ center at a neighbouring site. Thus, each chain termination will generate not less than 5 V^{5+} cations, which in the case of TC-30 corresponds to approximately 11% of the cation positions in the channels being vacant. This magnitude is not unreasonable considering that in a M2 containing some Nb, the number of Te–O vacancies was found to be 9.5% [17].

From the Te L_3-edge spectra in Fig. 7c it can be surmised that the bulk of the catalysts may contain besides Te^{4+} also some Te^{6+}, which is in line with the compositions of the catalysts being $Mo_{47}Te_3(V,Ti)_{25}(Te,Ce)_{25}O_{250}$ or $(Mo_{0.94}Te_{0.06})_2(V,Ti)_1(TeO,CeO)_1O_9$, i.e., with some Te in excess of the amount that is required for filling the hexagonal channels. The excess Te can be hexavalent and occupy some of the octahedral sites since 6-coordinated Te^{6+} and Mo^{6+} have similar ionic radii, which are 0.70 Å and 0.73 Å, respectively [36].

4.2 Surface Composition and Catalytic Functions

The quantitative XPS data in Table 2 reveal strong enrichment of Te and Ce on the catalyst surfaces, mainly at the expense of V and Ti. Also, the metal compositions do not change much after use of the catalysts in propene ammoxidation. It has previously been observed by XPS that M1/M2-type Mo–V–Nb–Te–O catalysts are enriched with Te at the surface on behalf of V [18, 39, 40], and the

same was observed for an M2-type phase with the composition $Mo_{3.33}V_{2.67}Te_2O_{20}$ [41]. Corresponding results were obtained when analyzing a M1-type Mo–V–Nb–Te–O sample with a highly surface sensitive LEIS system, showing for Te that the ratio between the topmost layer and the bulk was 2.7 [42]. Not only is the metal composition of the surfaces different from that of the bulk (Table 2), but so are the oxidation states as evidenced by comparing the XPS data in Table 2 and Figs. 3–6 with the corresponding XANES and ESR data in Figs. 7 and 14, respectively. Notable is that Te is hexavalent at the surface, whereas there are both Te^{4+} (channel sites) and Te^{6+} (octahedral sites) in the bulk. Moreover, for M2-0, VT-30 and VT-50, vanadium is pentavalent at the surface and tetravalent in the bulk. TC-30 shows V^{5+} on the surface and both V^{5+} and V^{4+} in the bulk. The connected presence of Te^{6+} and V^{5+} at the external parts of the catalysts can be explained by migration of Te from the channels, giving V^{5+} sites and supra-surface Te^{6+} sites. A hypothetical M2 with half-filled channels would correspond to the composition $(Te^{4+}O)_{0.5}Mo^{6+}{}_2\ V_1{}^{5+}O_9$.

The fact that the compositions and the oxidation states of the surfaces differ considerably from the bulk, suggests that the surface structure is different from that of the bulk. Calculations, assuming that 50% of the XPS signal comes from the topmost layer and the remaining 50% from a few layers beneath with the approximate bulk composition, although not necessarily the exact bulk structure, give an indication of the composition of the topmost layer. The compositions thus derived for M2-0, VT-30, VT-50 and TC-30 are $Mo_{34}V_1Te_{65}O_y$, $Mo_{35}V_4Ti_0Te_{61}O_y$, $Mo_{36}V_3Ti_0Te_{61}O_y$ and $Mo_{39}V_5Ce_{14}Te_{42}O_y$, respectively, indicating that the surfaces might consist mainly of Mo–Te(Ce)-oxide. Thus, the M2 bulk structure can be considered to be a support material for the active surface structure in agreement with previous proposals for M1-type Mo–V–Nb–Te-oxide [42, 43]. Additionally, the HRTEM images in Figs. 10–12 for M2-0, VT-30 and TC-30 indicate that the crystals, although well crystalline in the bulk, are terminated by a thin layer ($\sim$1–2 nm) of material without any visible long-range order. Similar results have previously been reported for both M1 and M2 [22, 44]. Interaction between the M2 bulk and the surface layer is clearly evidenced by the observation that the activity (Fig. 2) and the degree of reduction of Mo (Table 2) increases with the degree of Ti-substitution although the topmost layer practically does not contain any Ti. Actually, TeMoO and TeCeMoO mixed oxides supported on silica were studied for propene ammoxidation by Montedison already in the 1970's [45, 46]. The active phases in the two systems were believed to be Te_2MoO_7 [45] and, respectively, TeCeMoO [46] with the composition $Ce_4Mo_{11}Te_{10}O_{59}$ [47]. However, these catalysts were unstable and degraded during use, therefore never achieving commercial significance, in contrast to the Bi-molybdates that achieved great commercial success over now more than four decades [48]. Although the currently studied catalysts with a few layers of Mo–Te(Ce)-oxide on top of M2 crystallites were stable in the laboratory studies, their long-term stability has not been investigated. One may, however, speculate that they should be much more stable than neat Te-molybdates [45, 46] due to their bonding and interaction with the M2 phase.

The XPS data in Table 2 show reduction of Mo and Te upon use of the catalysts in ammoxidation, confirming that these are the two active elements in agreement with our indication that the active compositions essentially are TeMo-oxide and TeCeMo-oxide. According to the activity data in Fig. 2, the main effect of Ti substitution is to increase the specific activity of the catalyst. The XPS data in Table 2 show that the Te in the used VT-30 is considerably less reduced compared to Te in the unsubstituted M2-0. Thus, the increased activity is in agreement with a TeO site performing the rate limiting α-hydrogen abstraction from propene, and the reoxidation of the Te site by gaseous oxygen is improved due to bond adjustments through –Ti(base)–O···Te(surface) interaction, creating a Te site that is on a time average basis catalytically more efficient than a corresponding –V(base)–O···Te(surface) site. Since the amount of reduced Mo (Table 2) in the used VT-30 is higher than in the corresponding M2-0, it is a consequence of its higher activity. The observation that there is virtually no influence on the selectivity from reduced Mo suggests that Mo, like in other molybdate systems, is performing the nitrogen insertion (Mo=NH) and that this step is not rate limiting [12].

According to the activity data in Fig. 2, the main effect of Ce substitution for some of the Te is to increase the selectivity to acrylonitrile at the expense of acrolein, indicating that Ce addition affects the activation of ammonia. The XPS data in Table 2 for the used catalysts reveal that Ce improves the reoxidation of the catalyst; especially the reoxidation of Mo, and it also limits the reduction of Te by not forming Te^{2+}. The observation that the activity and the selectivity to acrylonitrile are higher for TC-30 than M2-0, is similar to the effects caused by Ce in other molybdate systems, which are induced by the reoxidation process $Ce^{4+} + Mo^{5+} \rightarrow Ce^{3+} + Mo^{6+}$ [46, 49, 50]. Our data for TC-30 indicate that a Mo site participates in the activation of ammonia to form a nitrogen inserting O=Mo=NH site, and further indicates that a Mo site surrounded by both Ce and Te is a better activator of ammonia than a corresponding site surrounded by Te only, which favours the creation of relatively more acrolein-forming O=Mo=O sites. Unlike the Te sites, Ce sites are not likely to perform the α-hydrogen abstraction from propene as it has been observed that the ammoxidation activity of

propene varies almost linearly with the Te content in α-(Ce,Te)O_2 [51]. The respective role of Te and Mo in the M2-type Mo–V(Ti)–Te(Ce)-oxide catalysts are largely identical to the functions indicated in previous work on propane ammoxidation on M1-type Mo–V–Nb–Te-oxide, where a V-site is the paraffin-activating site, a Te-site performs the α-hydrogen abstraction from the formed propene intermediate and the nitrogen insertion occurs on a Mo site; as originally proposed by Grasselli, Lopez-Nieto, Andersson [12–14, 18] and later also by Ueda [6].

5 Conclusions

Characterization of M2-type Mo–V(Ti)–Te(Ce)-oxide phases with XRD, HRTEM, XANES and ESR reveals that partial substitution of V with Ti and Te with Ce is possible.

XANES spectra show that Mo is hexavalent in the orthorhombic, pseudo-hexagonal M2-type bulk structure. Te is tetravalent in the hexagonal channel sites, whereas there may be also some hexavalent Te in the octahedral sites. In the unsubstituted M2 as in the Ti substituted analogues (7V/3Ti and 5V/5Ti), the V is tetravalent, as is also Ti in the latter samples. Conversely, in the Ce substituted sample (7Te/3Ce), the V K-edge XANES spectrum displays two types of V, and ESR analysis indicates the presence of both V^{5+} and V^{4+}. The Ce in the sample is trivalent.

XPS analysis shows for all samples that the composition of the surface region is quite different from the bulk. The surfaces are enriched with Te and also Ce when present, especially at the expense of V and Ti, indicating that the M2-type Mo–V(Ti)–Te–O and Mo–V–Te–Ce–O phases are essentially terminated by a layer of TeMo-oxide or TeCeMo-oxide, respectively. This indication is supported by HRTEM imaging, showing at the surfaces a 1–2 nm thick layer without any visible long-range ordering. Compared with the bulk, the valences of V and Te at the surface differ and are predominantly V^{5+} and Te^{6+}.

The M2-type phases are active and selective for propene ammoxidation, however, ineffective for propane ammoxidation as observed in separate experiments not reported here. Substitution of V with Ti results in improved propene ammoxidation activity, although the selectivities to acrylonitrile and acrolein largely are unaffected. Besides some improved activity, the main effect of Ce inclusion is to increase the selectivity to acrylonitrile at the expense of acrolein formation. From the XPS data of used catalysts it can be inferred that the improved activity caused by Ti substitution is due to its interaction with Te surface sites, thereby improving the reoxidation of the Te on the surface and thus participating indirectly in the rate limiting α-hydrogen abstraction from propene. The positive catalytic effect caused by Ce substitution is a consequence of the reoxidation process $Ce^{4+} + Mo^{5+} \rightarrow Ce^{3+} + Mo^{6+}$, facilitating the formation of nitrogen inserting O=Mo=NH moieties. Compared with a Mo site surrounded by Te only, a Mo site surrounded by both Ce and Te is a better activator of ammonia.

Acknowledgements R. Häggblad, J. Holmberg and A. Andersson acknowledge financial support from the Swedish Research Council. Prof. B.K. Hodnett and Mr. Balqzs Aszqlos-Kiss are acknowledged for their support with the surface analyses by making available the XPS machine at the University of Limerick (Ireland) as a part of the EU-funded Coordination Action CONCORDE.

References

1. Ushikubo T, Nakamura H, Koyasu Y, Wajiki S (1994) EP Patent 608 838, assigned to Mitsubishi Kasei Corporation, Tokyo, Japan
2. Botella P, Solsona B, Martinez-Arias A, López Nieto JM (2001) Catal Lett 74:149
3. Botella P, López Nieto JM, Solsona B, Mifsud A, Márquez F (2002) J Catal 209:445
4. Balcells E, Borgmeier F, Grißtede I, Linz H-G, Rosowski F (2004) Appl Catal A 266:211
5. Guiliants VV, Bhandari R, Al-Saeedi JN, Vasudevan VK, Soman RS, Guerrero-Pérez O, Bañares MA (2004) Appl Catal A 274:123
6. Ueda W, Vitry D, Katou T (2005) Catal Today 99:43
7. Baca M, Aouine M, Dubois JL, Millet JMM (2005) J Catal 233:234
8. Ushikubo T, Oshima K, Kayo A, Umezawa T, Kiyono K, Sawaki I (1992) EP Patent 529 853, assigned to the Mitsubishi Chemical Corporation, Tokyo, Japan
9. Komada S, Hinago H, Kaneta M, Watanabe M (1998) EP Patent 895 809, assigned to Asahi Kasei Kogyo Kabushiki Kaisha, Osaka, Japan
10. Vaarkamp M, Ushikubo T (1998) Appl Catal A 174:99
11. Ushikubo T (2000) Catal Today 57:331
12. Grasselli RK, Burrington JD, Buttrey DJ, DeSanto P Jr, Lugmair CG, Volpe AF Jr, Weingand T (2003) Top Catal 23:5
13. Oliver JM, López Nieto JM, Botella P (2004) Catal Today 96:241
14. Holmberg J, Grasselli RK, Andersson A (2004) Appl Catal A 270:121
15. Holmberg J, Häggblad R, Andersson A (2006) J Catal 243:350
16. Ushikubo T, Oshima K, Kayou A, Hatano M (1997) In: Li C, Xin Q (eds) Spillover and migration of surface species on catalysts. Elsevier, Amsterdam. Stud Surf Sci Catal 112:473–480
17. DeSanto P Jr, Buttrey DJ, Grasselli RK, Lugmair CG, Volpe AF Jr, Toby BH, Vogt T (2004) Z Kristallogr 219:152
18. Millet JMM, Roussel H, Pigamo A, Dubois JL, Jumas JC (2002) Appl Catal A 232:77
19. Baca M, Millet J-MM (2005) Appl Catal A 279:67; erratum (2005) 288:243
20. Botella P, López Nieto JM, Solsona B (2002) Catal Lett 78:383
21. Holmberg J, Hansen S, Grasselli RK, Andersson A (2006) Top Catal 38:17
22. Garcia-González E, López Nieto JM, Botella P, González-Calbet JM (2002) Chem Mater 14:4416
23. JCPDS International Centre for Diffraction data, Powder Diffraction File, Swarthmore, PA (1991)
24. Gaffney AM, Chaturvedi S, Clark MB Jr, Han S, Le D, Rykov SA, Chen JG (2005) J Catal 229:12
25. Andersson SLT, Järås S (1980) J Catal 64:51

26. Nilsson J, Landa-Cánovas AR, Hansen S, Andersson A (1999) J Catal 186:442
27. Huuhtanen J, Sanati M, Andersson A, Andersson SLT (1993) Appl Catal A 97:197
28. Salvi AM, Decker F, Varsano F, Speranza G (2001) Surf Interface Anal 31:255
29. Laachir A, Perrichon V, Badri A, Lamotte J, Catherine E, Lavalley JC, El Fallah J, Hilaire L, le Normand F, Quéméré E, Sauvion GN, Touret O (1991) J Chem Soc Faraday Trans 87:1601
30. Bak K, Hilaire L (1993) Appl Surf Sci 70/71:191
31. Holmberg J, Wagner JB, Häggblad R, Hansen S, Wallenberg LR, Andersson A (2007) Catal Today 128:153
32. Lin H-M, Kao S-T, Lin K-M, Chang J-R, Shyu S-G (2004) J Catal 224:156
33. Padežnik Gomilšek J, Kodre A, Bukovec N, Kozjek Škofic I (2004) Acta Chim Slov 51:23
34. Wu Z, Benfield RE, Guo L, Li H, Yang Q, Grandjean D, Li Q, Zhu H (2001) J Phys Condens Matter 13:5269
35. Nguyen DL, Ben Taarit Y, Millet JMM (2003) Catal Lett 90:65
36. Shannon RD (1976) Acta Crystallogr Sect A32:751
37. Magnéli A (1953) Acta Chem Scand 7:315
38. Filonenko VP, Grenthe C, Nygren M, Sundberg M, Zibrov IP (2002) J Solid State Chem 163:84
39. Holmberg J, Grasselli RK, Andersson A (2003) Top Catal 23:55
40. Feng R-M, Yang X-J, Ji W-J, Zhu H-Y, Gu X-D, Chen Y, Han S, Hibst H (2007) J Mol Catal A 267:245
41. Baca M, Pigamo A, Dubois JL, Millet JMM (2003) Top Catal 23:39
42. Guliants VV, Brongersma HH, Knoester A, Gaffney AM, Han S (2006) Top Catal 38:41
43. Guliants VV, Bhandari R, Brongersma HH, Knoester A, Gaffney AM, Han S (2005) J Phys Chem B 109:10234
44. Wagner JB, Timpe O, Hamid FA, Trunschke A, Wild U, Su DS, Widi RK, Hamid SBA, Schlögl R (2006) Top Catal 38:51
45. Bart JCJ, Giordano N (1980) J Catal 64:356
46. Bart JCJ, Giordano N (1984) Ind Eng Chem Prod Res Dev 23:56
47. Bart JCJ, Giordano N, Forzatti P (1985) In: Grasselli RK, Brazdil JF (eds) Solid state chemistry in catalysis, ACS Symp. Ser., vol 279. The American Chemical Society, Washington, DC, pp 89–101
48. Grasselli RK (2005) Catal Today 99:23; Grasselli RK, Tenhover MA (2008) In: Ertl G, Knözinger H, Schüth F, Weitkamp J (eds) Handbook of catalysis vol 8, 2nd edn., ch 14.11.9. Wiley-VCH Verlag GmbH & Co, p 3489
49. Brazdil JF, Grasselli RK (1983) J Catal 79:104; Brazdil JF, Glaeser LC, Grasselli RK (1983) J Phys Chem 87:5485; Grasselli RK (1985) Appl Catal 15:127
50. Giordano N, Bart JCJ, Maggiore R (1983) Kinet Katal 24:1140
51. Bart JCJ, Giordano N (1982) J Catal 75:134